© 2017. Published by The Company of Biologists Ltd | Development (2017) 144, 4313-4321 doi:10.1242/dev.155218

Single-cell mechanical phenotype is an intrinsic marker of reprogramming and differentiation along the mouse neural lineage

Marta Urbanska[1,*], Maria Winzi[1], Katrin Neumann[2], Shada Abuhattum[1,3], Philipp Rosendahl[1], Paul Müller[1], Anna Taubenberger[1], Konstantinos Anastassiadis[2] and Jochen Guck[1,*]

ABSTRACT

Cellular reprogramming is a dedifferentiation process during which cells continuously undergo phenotypical remodeling. Although the genetic and biochemical details of this remodeling are fairly well understood, little is known about the change in cell mechanical properties during the process. In this study, we investigated changes in the mechanical phenotype of murine fetal neural progenitor cells (fNPCs) during reprogramming to induced pluripotent stem cells (iPSCs). We find that fNPCs become progressively stiffer en route to pluripotency, and that this stiffening is mirrored by iPSCs becoming more compliant during differentiation towards the neural lineage. Furthermore, we show that the mechanical phenotype of iPSCs is comparable with that of embryonic stem cells. These results suggest that mechanical properties of cells are inherent to their developmental stage. They also reveal that pluripotent cells can differentiate towards a more compliant phenotype, which challenges the view that pluripotent stem cells are less stiff than any cells more advanced developmentally. Finally, our study indicates that the cell mechanical phenotype might be utilized as an inherent biophysical marker of pluripotent stem cells.

KEY WORDS: Cell mechanics, Pluripotency, iPSC, NPC, Real-time deformability cytometry, AFM

INTRODUCTION

Somatic cells can regain their pluripotency when forced to express a set of four defined transcription factors (Takahashi and Yamanaka, 2006). This cell identity change, called cellular reprogramming, is a dynamic remodeling process which has been widely characterized in terms of changes in gene expression patterns (Li et al., 2010; Samavarchi-Tehrani et al., 2010; Buganim et al., 2012; Polo et al., 2012; Hussein et al., 2014; Cacchiarelli et al., 2015), epigenetic landscape (Maherali et al., 2007; Lee et al., 2014a) or cytoskeletal organization (Sakurai et al., 2014; Boraas et al., 2016). However, little is known about how cell mechanical properties change during the process of reprogramming.

Mechanical properties, such as the Young's modulus, describe how much a cell deforms under a certain mechanical stress (force per unit area). If a cell is not deformed much by a given stress, it has a high Young's modulus and is considered stiff. Conversely, a cell that is deformed to a greater extent by the same stress has a lower Young's modulus, and is considered less stiff or more compliant (Lakes, 2009). The stiffness of a cell reflects its intracellular structure and is often tightly related to cell state and function. In the context of cell fate commitment, it has been shown with a variety of techniques that a change in cell stiffness is a sensitive indicator of cell differentiation, as in the case of the differentiation of murine embryonic stem cells (ESCs) (Chowdhury et al., 2010; Pillarisetti et al., 2011; Gossett et al., 2012), chondrogenic (Ofek et al., 2009) and cardiac (Tan et al., 2012) differentiation of human ESCs, osteogenic (Chen et al., 2010; Yu et al., 2010; Bongiorno et al., 2014) and adipogenic (Yu et al., 2010) differentiation of human mesenchymal stem cells, or differentiation of human myeloid precursor cells (Lautenschläger et al., 2009; Ekpenyong et al., 2012). Therefore, a dedifferentiation process such as reprogramming is potentially hallmarked by an alteration in cell stiffness.

In this study, we investigated changes in the mechanical phenotype of fetal neural progenitor cells (fNPCs) during the process of reprogramming to induced pluripotent stem cells (iPSCs) and, in reverse, the differentiation of iPSCs towards the neural lineage. For this purpose, we employed real-time deformability cytometry (RT-DC) – a robust and high-throughput technique allowing for rapid characterization of thousands of cells (Otto et al., 2015) – and confirmed the main findings with atomic force microscopy (AFM)-enabled nanoindentation, the gold standard in cell mechanical characterization. We find that fNPCs become progressively stiffer en route to pluripotency, and that, with the aid of CD24 and SSEA1 surface markers, mechanical subpopulations corresponding to differently advanced cells can be distinguished at intermediate reprogramming stages. Furthermore, we show that fNPC stiffening is mirrored by iPSCs becoming more compliant during differentiation towards the neural lineage, and that the mechanical phenotype of iPSCs is comparable with that of ESCs. These results suggest that the mechanical properties of cells are inherent to their developmental stage, and therefore might be important in guiding development. Our results also reveal that, at early developmental stages, pluripotent cells transition to a more compliant phenotype, which challenges the view that pluripotent stem cells are more compliant than any cells further advanced developmentally. Finally, this study indicates that the cell mechanical phenotype might be utilized as an inherent biophysical marker of pluripotent stem cells.

RESULTS

fNPCs stiffen during reprogramming to pluripotency

To elicit the transition towards pluripotency in a robust way, we used previously described fNPCs with an integrated Tet-On cassette

[1]Cellular Machines, Biotechnology Center, Center for Molecular and Cellular Bioengineering, Technische Universität Dresden, Tatzberg 47-49, Dresden 01307, Germany. [2]Stem Cell Engineering, Biotechnology Center, Center for Molecular and Cellular Bioengineering, Technische Universität Dresden, Tatzberg 47-49, Dresden 01307, Germany. [3]JPK Instruments AG, Colditzstraße 34-36, Berlin 12099, Germany.

*Author for correspondence (marta.urbanska@tu-dresden.de; jochen.guck@tu-dresden.de)

M.U., 0000-0002-6517-5958; M.W., 0000-0003-4925-5605; K.A., 0000-0002-9814-0559; J.G., 0000-0002-1453-6119

Received 22 May 2017; Accepted 24 October 2017

Development (2017) 144, 4313-4321 doi:10.1242/dev.155218

for doxycycline (dox)-inducible expression of the reprogramming factors Oct4 (Pou5f1), Sox2, Klf4 and cMyc (OSKM) (K. Neumann, PhD thesis, Technische Universität Dresden, 2014). fNPCs were induced to express the OSKM factors by addition of dox to the culture medium at day 0. Dox was kept at a constant concentration until day 19, after which it was removed from the medium. To guide reprogrammed cells towards the ground state of pluripotency, the medium was supplemented on day 14 with the two inhibitors PD0325901 and CHIR99021 (2i), targeting MEK1/2 (Map2k1/2) and GSK3α/β, respectively (Silva et al., 2008; Ying et al., 2008). From day 7 onwards, colony formation was visible as a first indicator of ongoing reprogramming (Fig. 1A). To verify successful and complete reprogramming, the expression of pluripotency-related genes, as well as neural markers, was evaluated and compared with the starting point of reprogramming (fNPCs). Using qRT-PCR analysis, we confirmed the upregulation of pluripotency genes such as *Nanog*, endogenous *Oct4* (*Oct4**), and *E-cadherin* (*Ecad*; or *Cdh1*), as well as the downregulation of neural markers expressed in fNPCs such as *Sox1*, *Nestin*, *Vimentin* (*Vim*) or *N-cadherin* (*Ncad*; or *Cdh2*) (Fig. 1B).

For the mechanical characterization of cells we used RT-DC (Otto et al., 2015), a novel microfluidic-based method that relies on deforming cells by hydrodynamic shear and normal stresses in a narrow constriction of a microfluidic chip (Mietke et al., 2015; Mokbel et al., 2017). The extent of deformation of cells is evaluated based on high-speed microscopy images. A custom image-

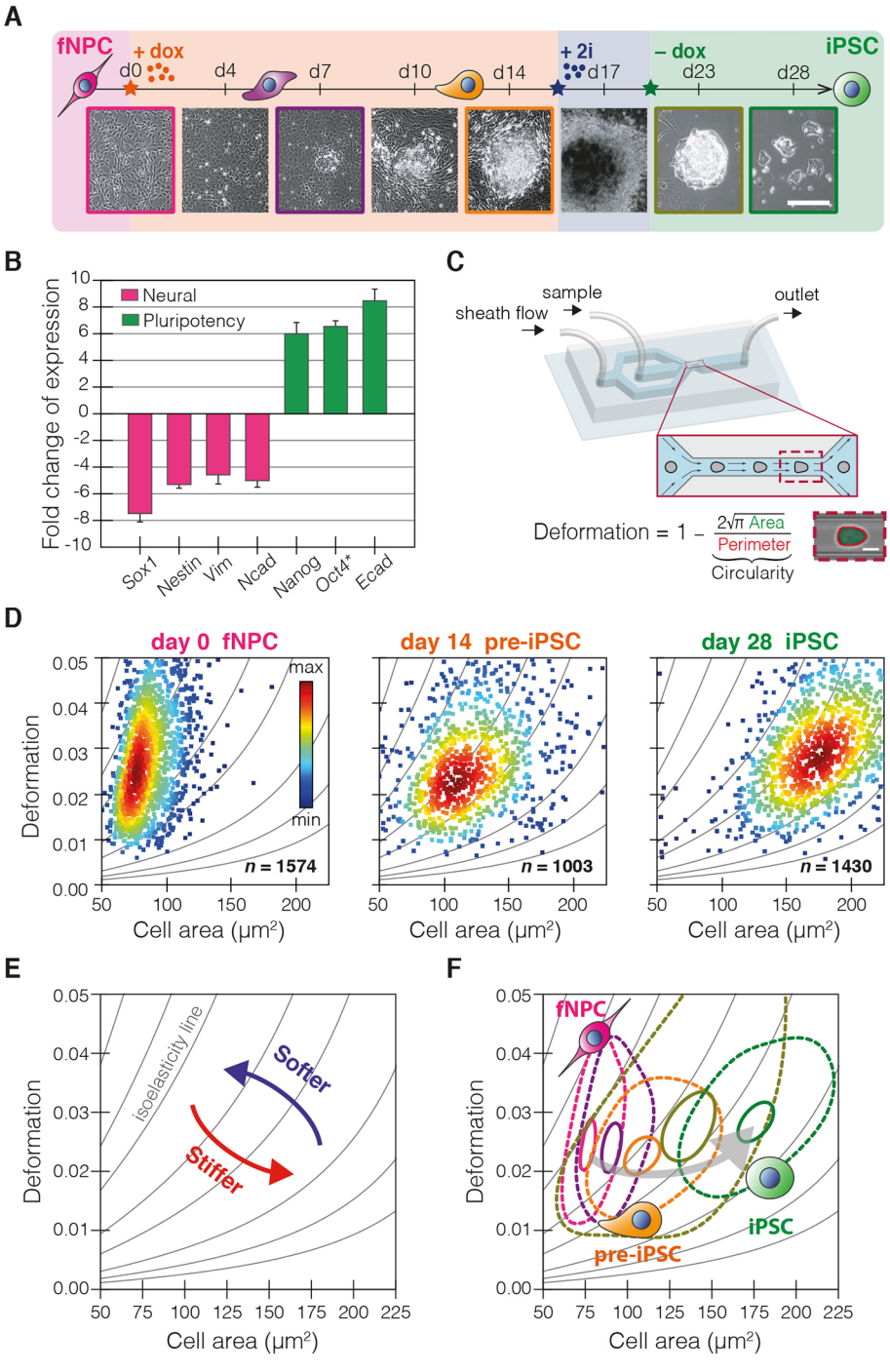

Fig. 1. fNPCs become progressively stiffer upon reprogramming to pluripotency. (A) Timeline of fNPC reprogramming and brightfield images presenting cell morphology during the reprogramming process. Scale bar: 200 µm. (B) Fold change in expression of neural and pluripotency-related markers at the end of reprogramming, as compared to fNPCs. Data are mean±s.d. from three independent experiments. (C) Operation principle of RT-DC. A microfluidic chip layout is shown in the background. In the foreground, the channel geometry with the indicated imaging region is depicted. The inset shows a picture of a deformed cell in the imaging region. Scale bar: 10 µm. (D) Deformation-cell area scatter plots showing populations of *n* cells on days 0, 14 and 28 of the reprogramming (from right to left). Color map indicates event density. (E) Deformation-cell area plot with isoelasticity lines from the analytical model for grouping cells with similar mechanical properties. (F) Color-coded 95%-density (solid lines) and 50%-density (dashed lines) contour plots of cells on days 0, 7, 14, 23 and 28 of reprogramming.

Development (2017) 144, 4313-4321 doi:10.1242/dev.155218

processing algorithm finds the cell contour and quantifies its deformation and projected area in real time (Fig. 1C). The results are then displayed on a deformation-cell area plot. On each day indicated in the timeline (Fig. 1A), a population of up to 1500 cells was characterized with RT-DC (Fig. S1A). The measurement results of three reference stages (day 0, 14 and 28) are displayed as scatter plots of deformation versus cell area in Fig. 1D.

Because larger cells experience higher stress in constriction, deformation is not a direct measure of cell stiffness. Therefore, an analytical model (Mietke et al., 2015) as well as numerical simulations (Mokbel et al., 2017) have been developed to provide reference isoelasticity lines for finding cells of different sizes with corresponding stiffness (Fig. 1E). Progression of the population characteristics is visualized with contour plots of populations at days 0, 7, 14, 23 and 28 (Fig. 1F), color-coded as in the schematics above (Fig. 1A). During the process of reprogramming, the population contours are crossing multiple isoelasticity lines towards the stiffer phenotype. This is also reflected by increasing median values of apparent Young's modulus, E, assigned to each cell based on measured cell size and deformation with interpolation of a data grid created by numerical simulations (Fig. S1B). The Young's modulus is a direct measure of cell stiffness and its knowledge facilitates comparing the mechanical phenotype of different cell states.

To confirm differences in the mechanical phenotype between fNPCs and iPSCs obtained by RT-DC, we performed indentation experiments on both rounded and adhering cells using AFM. Similar to the case of RT-DC analysis, the AFM data collected for both cell states show that iPSCs are significantly stiffer than fNPCs (Fig. S2).

Transgene-dependent F-class cells are more compliant than ESC-like iPSCs

If dox is not removed from the medium, the reprogrammed cells can stabilize at an alternative pluripotent state called F class (Fig. 2A) (Tonge et al., 2014). F-class cells are characterized by their dependence on ectopic expression of pluripotency factors, fast proliferation rate and cell contact-independent growth in fuzzy colonies, as opposed to compact colonies formed in the dox-independent ESC-like iPSC state (Fig. 2C). We found that F-class cells were more compliant than ESC-like iPSCs, as represented by a shift in their contour positions on the deformation-cell area plot (Fig. 2B), as well as by increased Young's modulus values determined from RT-DC measurements (Fig. 2D; Fig. S3A,B). According to the RT-DC data, fNPCs were significantly more compliant than cells of the F class (Fig. 2D). To validate these findings, we performed indentation experiments on rounded cells using AFM. The AFM data show, in accordance with RT-DC measurements, that F-class cells were significantly more compliant than transgene-independent iPSCs (Fig. 2E; Fig. S3C,D). However, the difference between fNPCs and F-class cells was not significant in AFM measurements (Fig. 2E).

Surface markers distinguish mechanical subpopulations at intermediate reprogramming stages

Regardless of the fact that colonies of reprogrammed cells started appearing among a population of cells with visually distinct morphology from day 7 onwards (Fig. 1A), it was not possible to clearly distinguish subpopulations solely on the basis of cell mechanics. To investigate whether such mechanical subpopulations corresponding to cells of different identities are present during the

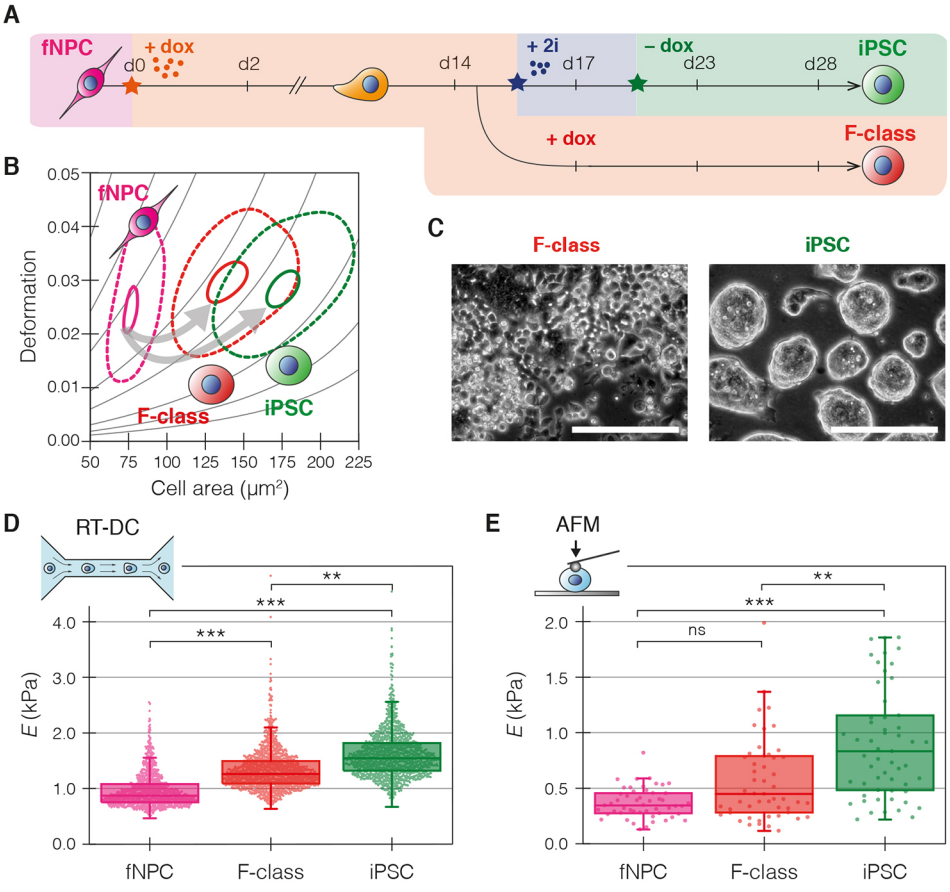

Fig. 2. Alternative pluripotent state shows a distinct mechanical phenotype. (A) Timeline of reprogramming leading to transgene-independent iPSCs (upper route) and transgene-dependent F-class cells (lower route). (B) Color-coded 95%-density (solid lines) and 50%-density (dashed lines) contour plots of fNPCs (reprogramming day 0), F-class cells and ESC-like iPSCs (after day 28). (C) Phase-contrast images presenting morphology of F-class cells (left panel) and ESC-like iPSCs (right panel). Scale bars: 200 µm. (D) Apparent Young's modulus E of fNPCs, F-class cell and iPSC populations measured in one RT-DC experiment (n=1238, 1502 and 1349, respectively). (E) Apparent Young's modulus E of fNPC, F-class cell and iPSC populations measured by AFM (n=51, 53 and 57, respectively). In D and E, boxes extend from the 25th to 75th percentiles, with a line at the median. Whiskers span 1.5× the interquartile range (IQR). ***P<0.001; **P<0.01; ns, not significant. Statistical analysis was performed using a linear mixed effects model on multiple experimental replicates. See Fig. S3 for all replicates.

Development (2017) 144, 4313-4321 doi:10.1242/dev.155218

reprogramming, we simultaneously monitored the mechanical properties and expression of two surface markers: SSEA1 and CD24. SSEA1 is a known early pluripotency marker (Brambrink et al., 2008; Samavarchi-Tehrani et al., 2010; Polo et al., 2012) and CD24 aids in distinguishing between dox-dependent F-class cells and dox-independent iPSCs (Shakiba et al., 2015). Using an integrated multichannel fluorescence readout and deformability measurement in a combined setup called real-time fluorescence and deformability cytometry (RT-FDC) (Rosendahl et al., 2017 preprint), we were able to acquire the surface marker expression and mechanical signature for each cell in one experiment.

We observed that fNPCs were positive for CD24 (CD24+) and negative for SSEA1 (SSEA1−) (Fig. S4A, day 0). Consistent with a previous report (Shakiba et al., 2015), a population of CD24 +/SSEA1+ cells started to emerge shortly after the addition of dox (Fig. S4A, day 4). Without subsequent withdrawal from dox, F-class cells stabilized in a CD24+/SSEA1+ state, whereas after withdrawal on day 19 the iPSCs stabilized in a CD24− state with moderate expression of SSEA1 (Fig. S4).

Interestingly, on day 23, a few days after withdrawal from dox, subpopulations of cells with different combinations of fluorescent marker expression are present (Fig. 3A). Using the marker expression, we were able to divide a seemingly unimodal cell distribution in the deformation versus cell area space from day 23 (Fig. 3B) into three subpopulations: NPC-like CD24+/SSEA1−, F-class-like CD24+/SSEA1+ and iPSC-like CD24−/SSEA1+/− (Fig. 3C). Next, we plotted the deformation versus cell area of the divided groups (Fig. 3D), and estimated the values of apparent Young's modulus (Fig. 3E). We found that the CD24+/SSEA1− cells were the most compliant, followed by CD24+/SSEA1+ cells corresponding to F-class cells, which have intermediate stiffness. All CD24− cells were stiffest and occupied a similar area in the deformation-cell area plot to the fully reprogrammed iPSCs (compare to Fig. 1E).

Neural differentiation of iPSCs mechanically mirrors reprogramming of NPCs

We next asked whether the change in the mechanical phenotype observed during reprogramming is unique to the direction of the reprogramming process, or is preserved in the process of reverse direction, that is, in neural specification. To test this, we induced neural differentiation of iPSCs and monitored the mechanical properties of the differentiating cells over time. iPSCs were plated at low density (≤10,000 cells per cm^2) and cultured in N2B27 medium (Fig. 4A), a condition sufficient to direct the cells towards the neural fate (Ying et al., 2003). To further facilitate differentiation towards neural precursor cells, epidermal growth factor (EGF) and fibroblast growth factor 2 (FGF2) were added when neural rosettes started to form on day 7 (Fig. 4A). Immunofluorescence staining of iPSCs before and after differentiation confirmed the successful formation of derived neural progenitor cells (dNPCs) after 12 days in differentiation medium (Fig. 4B). Although Sox2, a marker of pluripotency and neural fate, was expressed in iPSCs as well as dNPCs, dNPCs revealed a clear loss of the pluripotency marker Nanog and upregulation of the neural-specific transcription factor Pax6 (Fig. 4B).

Mechanical phenotyping by RT-DC showed that the cells became smaller and more compliant over the time course of differentiation (Fig. 4C,D; Fig. S5). A direct comparison of the Young's modulus, *E*, between reprogramming and differentiation showed unambiguously that dNPCs, similar to fNPCs, are significantly more compliant than iPSCs (Fig. 4E).

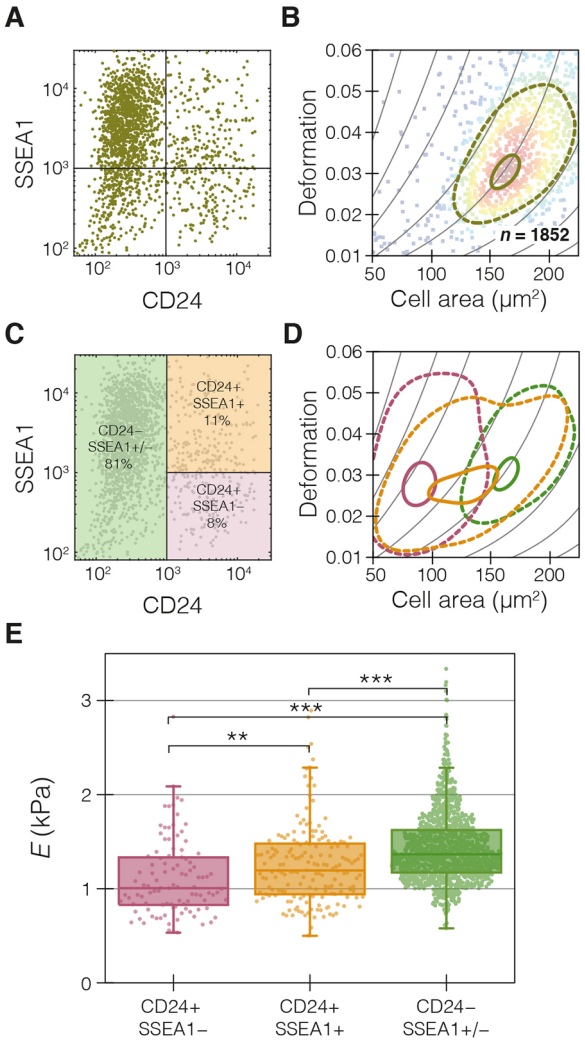

Fig. 3. CD24/SSEA1 staining reveals mechanical subpopulations on day 23 of reprogramming. (A) CD24 versus SSEA1 expression of 1852 cells on day 23 of reprogramming (after dox withdrawal), analyzed by RT-FDC. (B) Area and deformation recorded for the population of cells from A. (C) Three gates for dividing the cells into three groups based on CD24/SSEA1 expression. The % values indicate the fraction of cells in each gate on day 23. (D) Color-coded 95%-density (solid lines) and 50%-density (dashed lines) contour plots of deformation versus cell area for the cell population from B subdivided into three groups: CD24+/SSEA1− (purple, *n*=148), CD24 +/SSEA1+ (orange, *n*=203) and CD24-/SSEA1+/− (green, *n*=1500). (E) Apparent Young's modulus *E* determined from the RT-DC data for the cell subpopulations specified above. Boxes extend from the 25th to 75th percentiles, with a line at the median. Whiskers span 1.5× the IQR. ***P<0.001; **P<0.01. Statistical significance was determined with the Mann–Whitney test.

Mechanical phenotype from NPCs to pluripotency

Finally, we compared all the measured cell states from those most advanced developmentally towards the neural lineage to those least advanced and most pluripotent. The cell states include fNPCs, dNPCs, F-class cells and iPSCs presented above, and additionally measured epiblast stem cells (EpiSCs) and ESCs (Fig. 4F). Strikingly, we observed that the more pluripotent the cell state, the higher the Young's modulus it exhibits. Noteworthy, the measurements show that iPSCs and ESCs are comparably stiff (see also Fig. S6), indicating that mechanical phenotype is a marker of pluripotency shared between these two cell types.

Development (2017) 144, 4313-4321 doi:10.1242/dev.155218

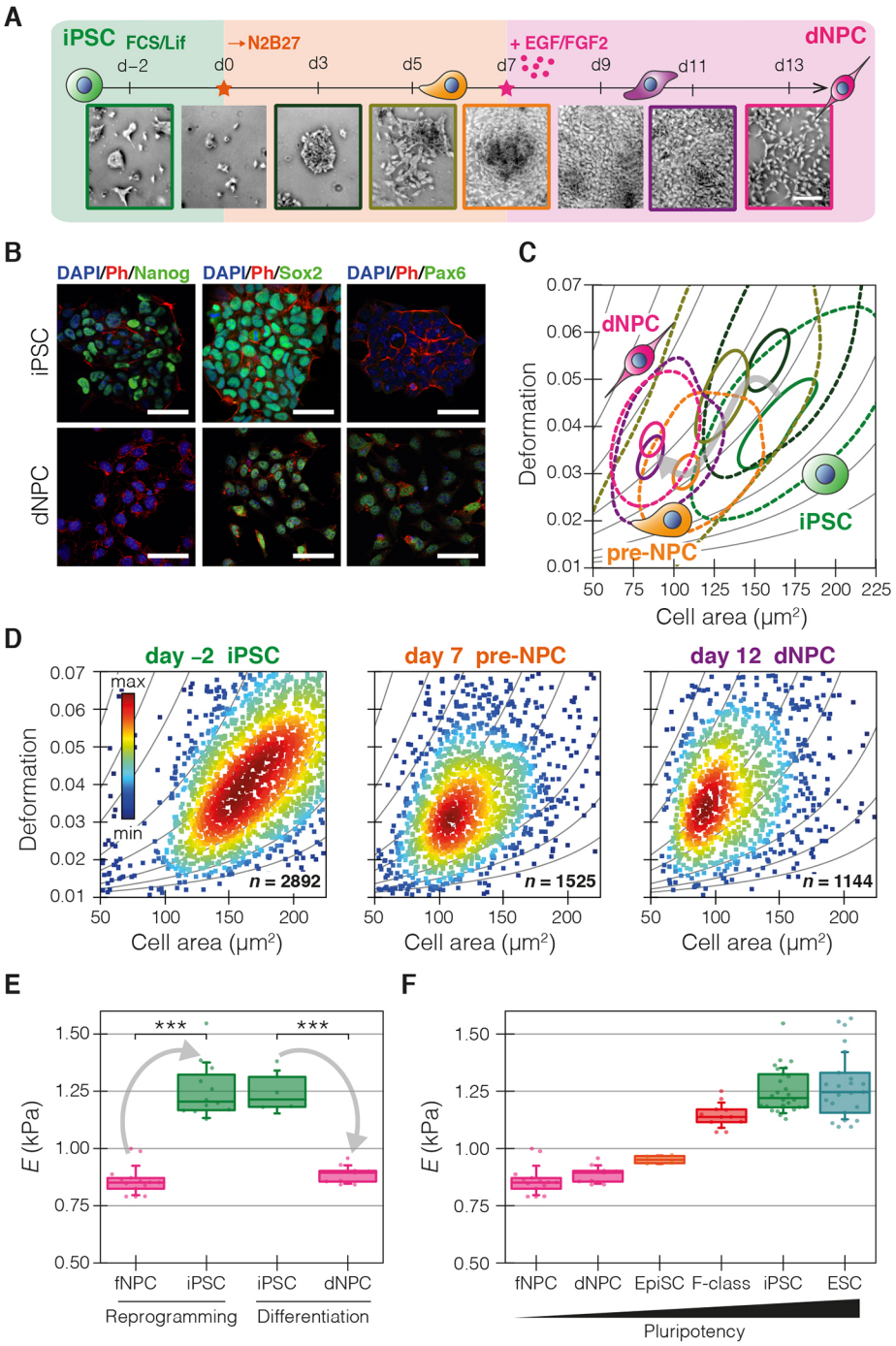

Fig. 4. iPSCs become more compliant while differentiated towards the neural lineage. (A) Timeline of iPSC differentiation towards dNPCs, and phase-contrast images presenting cell morphology along the differentiation process. Scale bar: 200 µm. (B) Immunofluorescence staining for Nanog, Sox2 and Pax6 at the beginning (iPSC) and end (dNPC) of the differentiation. Ph, Phalloidin. Scale bars: 50 µm. (C) Color-coded 95%-density (solid lines) and 50%-density (dashed lines) contour plots of cells on days 2, 3, 5, 7, 11 and 13 of the differentiation. (D) Deformation-cell area scatter plots showing populations of *n* cells on days 2, 8 and 12 of the differentiation (from right to left). Color map indicates event density. (E) Apparent Young's modulus *E* derived from the RT-DC data for the terminal stages of reprogramming and differentiation. (F) Apparent Young's modulus *E* derived from the RT-DC data for cells representing different developmental stages from NPCs to ESCs. In E and F, each data point represents the median of an individual RT-DC measurement. Boxes extend from the 25th to 75th percentiles, with a line at the median. Whiskers indicate s.d. ***$P<0.001$. Statistical analysis was performed using a linear mixed effects model.

DISCUSSION

Mechanical forces are becoming increasingly recognized as important factors driving cell and tissue morphogenesis (Mammoto and Ingber, 2010; Heisenberg and Bellaïche, 2013; Davidson, 2017). To further understand the contributions of forces during development, detailed studies on the biomechanical aspects of cell fate commitment and identity changes are indispensable. Here, we characterized, on a population level, how the mechanical properties of cells are changing during the process of acquiring new identity in an *in vitro* setting. In particular, we examined with the microfluidics-based RT-DC technique the transition from fNPCs to iPSCs in the reprogramming process, and found that this conversion is accompanied by cell stiffening. We could also show that, in the converse process of neural differentiation, iPSCs become more compliant and retrieve the fNPC phenotype. The trend of fNPCs being more compliant than iPSCs was confirmed by AFM measurements on rounded as well as adherent cells. Remarkably, by comparing multiple cell types of different pluripotency levels – from the least potent fNPCs through EpiSCs and F-class cells to the most pluripotent iPSCs and ESCs – we identified that the more pluripotent the cell identity, the stiffer the cells appear.

Contrary to our results, murine ESCs have previously been reported to be more compliant than their differentiated progeny (Chowdhury et al., 2010; Pillarisetti et al., 2011; Gossett et al., 2012). In each of those studies, different culture conditions, resulting in the derivation of diverse lineages, were used. In the

Development (2017) 144, 4313-4321 doi:10.1242/dev.155218

case of Pillarisetti et al. (2011), mesodermal differentiation was induced, whereas Chowdhury et al. (2010) and Gossett et al. (2012) investigated heterogeneous populations of differentiated progeny, consisting, most likely, of cells from all three germ layers. None of the differentiation methods used corresponds to the procedure used in our study, which directs the cells exclusively towards neural lineage. Furthermore, the discrepancies in the results obtained can be attributed to different stiffness-probing strategies. Chowdhury et al. (2010) have used optical magnetic twisting cytometry to probe cell stiffness. This method relies on twisting magnetic beads anchored to the cytoskeleton via focal adhesions, which first corresponds to probing the local attachment sites rather than global cell mechanics, and second, might reflect on other properties of cells, such as their ability to form focal adhesions. Pillarisetti et al. (2011) have used AFM to probe mechanical changes in differentiated cells in adherent cell exclusively. Gossett et al. (2012) have employed deformability cytometry (DC), which, similar to RT-DC, relies on measuring single cells in suspension. However, the probing timescales and applied forces vary substantially between these two methods. That leads to sensitivity to different intracellular features. In DC, cells are deformed within a few microseconds by forces >1 µN (Gossett et al., 2012), a condition believed to cause filament fluidization. Such fluidization is reflected by low sensitivity of DC to drugs disrupting the cytoskeletal elements (Gossett et al., 2012). Thus, DC seems to be primarily sensitive to nuclear mechanics and cytoplasmic contribution to cell stiffness. The observation of cell stiffening during differentiation in DC could, therefore, be attributed to the previously described phenomenon of increased nuclear stiffness in differentiated cells (Pajerowski et al., 2007). RT-DC, in turn, deforms cells within a few milliseconds with sub-µN forces, and was recently shown to be primarily sensitive to cytoskeletal perturbations, in particular to those related to the actin cytoskeleton (Golfier et al., 2017).

Future work will be necessary to identify molecular and structural features underlying the mechanical differences between iPSCs and fNPCs reported in this study. Features such as organization of the cytoskeleton, specifically the F-actin cytoskeleton, its anchorage to the membrane and the nucleus, its contractile activity, nuclear-to-cytoplasmic ratio and mass density of the cytoplasm, are examples of potential factors that could be tested. Furthermore, it would be interesting to evaluate whether the changes in cell stiffness during reprograming are reflected by activity of the transcriptional co-regulators YAP (YAP1) and TAZ. YAP and TAZ are prominent players in mechanotransduction cascades and change their localization from cytoplasmic to nuclear upon mechanical stimulation (Panciera et al., 2017). Interestingly, YAP has been shown to play a role in rigidity-dependent differentiation of human iPSCs towards the neural lineage (Musah et al., 2014; Sun et al., 2014), and in cell fate specification in the preimplantation stage mouse embryo (Nishioka et al., 2009; Maître et al., 2016). Additionally, transient expression of YAP/TAZ was recently shown to turn differentiated cells into tissue-specific stem/progenitor cells, which highlights the importance of mechanosensing for cell stemness (Panciera et al., 2016).

Cell stiffness is an intrinsic property of individual cells and therefore holds the promise of serving as a label-free marker of cell state with great translational potential (Di Carlo, 2012). In combination with other biophysical markers, cell stiffness was shown to be predictive of mesenchymal stromal cell multipotency *in vivo* as well as after *in vitro* expansion (Lee et al., 2014b). According to our results, cell stiffness is associated with pluripotency in mice and could be used to identify and enrich pluripotent cells in mixed populations. From a clinical point of view, it is essential that, at the end of reprogramming to pluripotency, a homogenous cell population of fully reprogrammed bona fide iPSCs is obtained. Even though there is a multitude of known biochemical markers associated with pluripotency in mice (Brambrink et al., 2008) and human (Adewumi et al., 2007; Ohnuki et al., 2009), most of them require either sacrification of cells (e.g. alkaline phosphatase staining) or introduction of a labeling agent (antibodies against surface markers such as SSEA1 in mice or SSEA3 and SSEA4 in human). As demonstrated by the stiffening of cells during reprogramming and the presence of various mechanical populations at the intermediate stages of reprogramming, cell stiffness could be a valuable label-free marker for selecting fully reprogrammed, pluripotent cells from heterogeneous populations without jeopardizing their viability (Otto et al., 2015). Because in RT-DC deformation is evaluated in real time, the method is highly compatible with online sorting. There are several microfluidics-based passive and active sorting mechanisms (Zhu and Trung Nguyen, 2010) that could be implemented downstream to the analysis in an RT-DC setup. This would open up opportunities for not only enriching cells of selected stiffness for translational purposes, but also for investigating the molecular basis of mechanical differences in cell subpopulations.

Cell mechanics, apart from being an indicator of cell fate transitions, also plays an active role in guiding development (Wozniak and Chen, 2009). For example, it has recently been shown that cell contractility drives the first lineage decision in the developing mouse embryo (Maître et al., 2016). Additionally, the stiffness of individual cells contributes to the biomechanical surroundings perceived by neighboring cells. Mechanical cues can, in turn, influence the fate of cells (Guilak et al., 2009; Yim and Sheetz, 2012). The environment stiffness has been shown to determine the fate of human mesenchymal stem cells (Engler et al., 2006) or orchestrate Wnt protein-dependent mesodermal differentiation of human ESCs (Przybyla et al., 2016). Efforts invested in mechanical characterization of individual cells at different developmental stages will contribute to better understanding of local mechanical setting in the embryo. In the future, with the aid of noninvasive techniques for measurement of cell and tissue mechanics such as Brillouin microscopy (Scarcelli et al., 2015), these cell-level findings could be verified by mechanical *in situ* measurements in the context of the developing organism.

The stiffness of tissues and individual cells reflect their function. Load-bearing tissues, such as bone, cartilage or skeletal muscle, exhibit a high elastic modulus, other tissues that are not load bearing, such as breast or brain, are characterized by low elastic moduli (Handorf et al., 2015). Similarly, at the level of single cells, osteocytes have been reported to be much stiffer than chondrocytes or adipocytes (Darling et al., 2008; Yu et al., 2010), and glial and neuron cells have been reported to be much more compliant than other cells (Lu et al., 2006). In the light of this knowledge, the transition from a stiffer to a more compliant phenotype in the case of neural differentiation is justified from a functional point of view. While cells in the early embryo should exhibit resistance to mechanical forces and remain robust, the differentiating cells at gastrulation stage have to be able to reorganize and migrate to new locations. The migratory, invasive phenotype is often related to a compliant phenotype, as for example in cancer metastasis (Guck et al., 2005; Xu et al., 2012). Upon further differentiation towards the neural lineage, cells should acquire the mechanical phenotype

Development (2017) 144, 4313-4321 doi:10.1242/dev.155218

corresponding to that of the target tissue, which, as discussed above, is reported to be compliant.

Taken together, our findings establish a defined mechanical phenotype associated with the state of pluripotency that is shared by ESCs and iPSCs. In relation to the neural lineage specification, this phenotype appears stiff. Further studies analyzing the differentiation towards mesodermal and endodermal lineages will be necessary for creating a complete mechanical landscape of murine stem cell specification, and will contribute to understanding the role of cell mechanics in cell fate commitment.

MATERIALS AND METHODS

Cell culture

fNPCs were isolated from the telencephalon of embryonic day (E) 15.5 mouse embryos (strain C57BL/6J) as described elsewhere (K. Neumann, PhD thesis, Technische Universität Dresden, 2014) and cultured in NPC medium [Euromed-N (Biozol), 1× N2 supplement (Gibco), 0.5× B27 supplement (Gibco), 2 mM L-glutamine, 10 ng/ml EGF (Peprotech), 10 ng/ml recombinant FGF2 (MPI-CBG)] on dishes coated with laminin (2 µg/ml, Sigma-Aldrich). Passaging was performed using accutase (Sigma-Aldrich).

ESCs were established from E3.5 blastocysts (strain C57BL/6J) as previously reported (K. Neumann, PhD thesis, Technische Universität Dresden, 2014) and cultured on 0.1% gelatin-coated dishes in FCS/LIF medium [DMEM+Glutamax (Gibco), 15% fetal calf serum (Pansera ES, PAN-Biotech), 100 µM β-mercaptoethanol (PAN-Biotech), 2 mM L-glutamine (Gibco), 1 mM sodium pyruvate (Gibco), 1× nonessential amino acids (Gibco), 15 ng/ml recombinant LIF (MPI-CBG)] with or without a mixture of MEK inhibitor PD0325901 (1 µM) and GSK3 inhibitor CH99021 (3 µM) known as 2i. Cells were passaged using 0.1% trypsin solution.

EpiSCs were derived from ESCs as described previously (Guo et al., 2009), and cultured in N2B27 medium [50% DMEM/F12, 50% Neurobasal medium (Gibco), 0.5× B27 supplement (Gibco), 0.5× N2 supplement (Gibco), 2 mM L-glutamine (Gibco), 100 µM β-mercaptoethanol (PAN-Biotech)] supplemented with 12 ng/ml recombinant FGF2 (MPI-CBG) and 30 ng/ml Activin A (MPI-CBG) on dishes coated with fibronectin (10 µg/ml, Millipore). Passaging was performed using accutase (Sigma-Aldrich).

Reprogramming of fNPCs into iPSCs

The Tet-On system for dox-inducible expression of OSKM factors in fNPCs was established as previously described (K. Neumann, PhD thesis, Technische Universität Dresden, 2014). In brief, fNPCs were first nucleofected with CAG-rtTA-IRES-neo plasmid according to the manufacturer's instructions (Lonza, VPG-1004) and selected with 200 µg/ml G418. Then, functionally selected clones were nucleofected with circular PB-tetCMV-OSKM-puro and CMV-PBase-neo and selected with 1.0 µg/ml puromycin.

For reprogramming, the irtTA-neo PB-tetCMV-OSKM fNPCs were seeded on dishes coated with laminin at a density of 35-70×10^5 per cm^2 in NPC medium with 1 µg/ml of doxycycline (Sigma-Aldrich). After 2 days, the NPC medium was replaced with FCS/LIF medium. The medium was refreshed daily. For obtaining iPSCs, a mixture of MEK inhibitor PD0325901 (1 µM) and the GSK3 inhibitor CH99021 (3 µM) known as 2i was supplemented to the medium on day 14, and on day 17, dox was removed from the medium. For derivation of F class, neither 2i addition nor dox withdrawal was performed. The iPSCs were further cultured on gelatin-coated dishes.

Neural differentiation of iPSCs

For neural differentiation, iPSCs were seeded on 0.1% gelatin-coated dishes at a density of 5-10×10^5 per cm^2 in FCS/LIF medium without 2i. After overnight incubation, the medium was changed to N2B27. The medium was exchanged daily and on day 7 supplemented with 10 ng/ml EGF (Peprotech) and 10 ng/ml recombinant FGF2 (MPI- CBG). On day 10 or 11, cells were detached using accutase and cultured over a few more passages in EGF/FGF2-supplemented N2B27 medium on gelatin-coated dishes.

RT-DC

A PDMS microfluidic chip was placed on a microscope (Axiovert200 M, Zeiss) and filled with MC-PBS [high-viscosity (15 mPa s) PBS solution containing 0.5% (w/v) methylcellulose (Alfa Aesar)] with the aid of a syringe pump (NemeSys, Cetoni). Prior to an RT-DC experiment, cells were detached from culture plates, centrifuged and resuspended in MC-PBS at a concentration of 0.5-4×10^6 cells per ml. The cell suspension was then aspirated into a polymer (PEEK) tubing attached to a syringe and introduced into the microfluidic chip. Cells were flown into the narrow channel constriction (20×20 µm square cross-section, 300 µm length) under a constant flow rate of 0.04 µl/s. Data acquisition was performed at room temperature (~23°C) in a 85×27 µm region of interest at the end of the flow channel with a high-speed CMOS camera (MC1362, Mikrotron) operating at 2000 fps. For stroboscopic illumination, an LED-based light source synchronized to the camera (Accellerator L1, Zellmechanik Dresden) was used. The imaging was performed through an EC Plan-Neofluar 40×/0.75 NA objective (Zeiss). The cell deformation and cell area were determined in real time by an image-processing algorithm implemented in a combination of C++ (Microsoft) and LabVIEW (National Instruments), as previously described (Otto et al., 2015). Typically 2000-4000 cells were analyzed in one experiment. For plotting and further analysis, data were filtered for 50-500 $µm^2$ cell area and 1.00-1.05 area ratio. Area ratio is defined as the ratio between the area enclosed by the convex hull of the contour and the area enclosed by the contour. Area-deformation scatter plots and contour plots were generated using the analysis software ShapeOut version 0.7.3 (available at https://github.com/ZELLMECHANIK-DRESDEN/ShapeOut).

The apparent Young's modulus, *E*, was determined in a postprocessing step using a data grid obtained from numerical simulations for an elastic solid (Mokbel et al., 2017) with the aid of ShapeOut 0.7.3. We describe the determined Young's modulus as apparent, owing to the fact that some of the assumptions required for the theoretical modeling (e.g. cells being homogenous elastic objects) are not fully satisfied.

For combined assessment of surface marker expression and deformation, an RT-FDC setup with integrated fluorescence detection was used (Rosendahl et al., 2017). Prior to the measurements, cells were stained for 10 min with Anti-SSEA-1-APC (1:10, REA321, Miltenyi Biotec) and CD24-FITC (1:10, M1/69, Miltenyi Biotec) antibodies in a 0.3% BSA solution in PBS. Fluorescence excitation was performed using 488 nm and 640 nm laser lines (OBIS, Coherent Deutschland). Collected emission was spectrally separated into two detection channels using band-pass filters (525/50 nm and 700/75 nm) and individually registered with avalanche photodiode detectors (MiniSM10035, SensL Corporate). For marker expression analysis peak maxima were used as a parameter describing fluorescence intensity.

AFM

AFM-enabled nanoindentation experiments were performed using the Nanowizard 1 and 4 setups (JPK Instruments AG). A 5 µm polystyrene bead (microParticles) was glued to the end of each tip-less silicone cantilever with a force constant in the range 0.35-0.45 N/m (Arrow TL1, Nanoworld) and used as the indenter. Cantilever calibration was performed with the thermal noise method. Measurements were performed in a CO_2-independent medium (Gibco) at a constant temperature of 37°C. For experiments on rounded cells, cells were detached using 0.1% trypsin solution, placed onto a glass-bottomed petri dish (FD35100, World Precision Instruments) and allowed to settle onto the surface for ~10 min before starting the measurements. For experiments on adherent and spread cells, cells were plated on glass-bottom petri dishes and allowed to adhere overnight. The indenter was placed roughly at the center of each cell (Fig. S2E,F). Indentation onto the cell surface was performed with the extension speed of 5 µm/s to a maximum force of 2 nN. Recorded force-distance curves were converted into force-indentation curves and analyzed with JPK data processing software (JPK Instruments AG) using Sneddon's modification of the Hertz model for a spherical indenter (Sneddon, 1965). The force-indentation curves were fitted to a maximal indentation of 1.5 µm. A Poisson ratio of 0.5 was assumed. The obtained apparent Young's modulus values, *E*, were corrected with (i) an effective probe radius for the case of contact between two spherical objects, and (ii) a simplified double contact model (Glaubitz et al., 2014), accounting for compression arising from

Development (2017) 144, 4313-4321 doi:10.1242/dev.155218

contact with the substrate at the bottom part of the cell. We refer to the obtained Young's modulus values as apparent because some of the theoretical assumptions used for the implemented models are not fully satisfied in our setup; for example, we cannot assume that measured cells are fully homogenous and purely elastic.

qRT-PCR

Total RNA was isolated using an Aurum Total RNA Mini Kit (Bio-Rad), including a DNase treatment directly on the column. For each reaction, 1 µg of RNA was reverse transcribed using a High-Capacity cDNA Reverse Transcription Kit (ThermoFisher Scientific), utilizing MuLV reverse transcriptase and random primers. SYBR Green-based quantitative PCRs were run with the Absolute qPCR Mix (ThermoFisher Scientific) on an Mx3000 qRT-PCR system (Stratagene). Measured transcript levels were normalized to *Tbp*. Samples were run in duplicate. For each condition, three samples from different cell passages were collected. The sequences of primers used and the lengths of obtained products are summarized in Table S1. The fold change in expression levels was calculated as $\log_2$ of the ratio of the expression levels in iPSCs to the expression levels in the reference stage (fNPCs).

Immunofluorescence staining

For immunofluorescence, 50,000 cells per well were seeded in ibiTreat eight-well µ-slides (ibidi), cultured for 1-2 days and fixed for 10 min with 4% paraformaldehyde. Permeabilization and blocking were performed for 30 min in PBS containing 0.3% Triton-X and 10% fetal calf serum. Next, staining with primary antibodies [anti-Nanog (1:200, RCAB002P-F, Reprocell), anti-Sox2 (1:100, AB5603, Merck Millipore) and anti-Pax6 (1:10, DSHB)] was performed overnight at 4°C in staining solution (0.3% Triton-X in PBS). In the second staining step, the sample was incubated with the staining solution containing Cy2-conjugated donkey secondary antibodies (1:500, Jackson ImmunoResearch), DAPI (1:5000, D1306, Molecular Probes), and Phalloidin-TRITC (1:500, P1951, Sigma-Aldrich) for 30 min at room temperature. Imaging was performed on an inverted confocal laser scanning microscope (LSM700, Zeiss) using a Plan-Apochromat 20×/0.8 NA air objective (Zeiss).

Statistical analysis

To perform statistical analysis on multiple sets of experiments, linear mixed effects models were implemented using the lme4-package in R (R Core Team, 2017; www.R-project.org/.). The model included two fixed effects and one random effect. The fixed effects were attributed to the cell type and the experiment series; the random effect was attributed to the measurement day. Adjustments of both the slope and intercept were allowed for the random effect. *P*-values were obtained by performing a likelihood ratio test comparing the model with a null model lacking the fixed effect attributed to the cell type.

In the case of a single data set, statistical analysis was performed using the Mann–Whitney test, implemented in Origin 2015 software (OriginLab, www.originlab.com/).

Acknowledgements

We thank the Light Microscopy Facility and the Microstructure Facility at the Center for Molecular and Cellular Bioengineering (CMCB) at Technische Universität Dresden for excellent support and help with the production of RT-DC chips, respectively. We are grateful to Isabel Richter for technical assistance, Oliver Otto for fruitful discussions and methodological support, and Maik Herbig for support with statistical analysis. The Pax6 antibody was acquired from the Developmental Studies Hybridoma Bank, developed under the auspices of the Eunice Kennedy National Institute of Child Health and Human Development (NICHD) and maintained by The University of Iowa, Department of Biological Sciences, Iowa City, IA.

Competing interests

P.R. is a co-founder and head of product development of Zellmechanik Dresden, a company commercializing real-time deformability cytometry technology. P.R. and P.M. are employees of Zellmechanik Dresden. All other authors state no competing interests.

Author contributions

Conceptualization: M.U., M.W., K.N., K.A., J.G.; Methodology: M.U., M.W., K.N., S.A., P.R., A.T., K.A., J.G.; Software: M.U., P.R., P.M.; Formal analysis: M.U., S.A., A.T.; Investigation: M.U., M.W.; Resources: K.N., K.A., J.G.; Writing - original draft: M.U.; Writing - review & editing: M.U., M.W., K.N., P.R., K.A., J.G.; Visualization: M.U.; Supervision: M.W., K.N., K.A., J.G.; Project administration: M.U.; Funding acquisition: J.G.

Funding

This work was supported by Alexander von Humboldt-Stiftung (Alexander von Humboldt Professorship to J.G.) and the European Commission through the BIOPOL ITN (Marie Skłodowska-Curie Action of the Horizon 2020 program; 607350). The facilities of the CMCB are partly funded by the State of Saxony and the European Regional Development Fund.

Supplementary information

Supplementary information available online at
http://dev.biologists.org/lookup/doi/10.1242/dev.155218.supplemental

References

Adewumi, O., Aflatoonian, B., Ahrlund-Richter, L., Amit, M., Andrews, P. W., Beighton, G., Bello, P. A., Benvenisty, N., Berry, L. S., Bevan, S. et al. (2007). Characterization of human embryonic stem cell lines by the International Stem Cell Initiative. *Nat. Biotechnol.* **25**, 803-816.

Bongiorno, T., Kazlow, J., Mezencev, R., Griffiths, S., Olivares-Navarrete, R., McDonald, J. F., Schwartz, Z., Boyan, B. D., McDevitt, T. C. and Sulchek, T. (2014). Mechanical stiffness as an improved single-cell indicator of osteoblastic human mesenchymal stem cell differentiation. *J. Biomech.* **47**, 2197-2204.

Boraas, L. C., Guidry, J. B., Pineda, E. T. and Ahsan, T. (2016). Cytoskeletal expression and remodeling in pluripotent stem cells. *PLoS ONE* **11**, 1-16.

Brambrink, T., Foreman, R., Welstead, G. G., Lengner, C. J., Wernig, M., Suh, H. and Jaenisch, R. (2008). Sequential expression of pluripotency markers during direct reprogramming of mouse somatic cells. *Cell Stem Cell* **2**, 151-159.

Buganim, Y., Faddah, D. A., Cheng, A. W., Itskovich, E., Markoulaki, S., Ganz, K., Klemm, S. L., Van Oudenaarden, A. and Jaenisch, R. (2012). Single-cell expression analyses during cellular reprogramming reveal an early stochastic and a late hierarchic phase. *Cell* **150**, 1209-1222.

Cacchiarelli, D., Trapnell, C., Ziller, M. J., Soumillon, M., Cesana, M., Karnik, R., Donaghey, J., Smith, Z. D., Ratanasirintrawoot, S., Zhang, X. et al. (2015). Integrative analyses of human reprogramming reveal dynamic nature of induced pluripotency. *Cell* **162**, 412-424.

Chen, Q., Xiao, P., Chen, J.-N., Cai, J.-Y., Cai, X.-F., Ding, H. and Pan, Y.-L. (2010). AFM studies of cellular mechanics during osteogenic differentiation of human amniotic fluid-derived stem cells. *Anal. Sci.* **26**, 1033-1037.

Chowdhury, F., Na, S., Li, D., Poh, Y.-C., Tanaka, T. S., Wang, F. and Wang, N. (2010). Material properties of the cell dictate stress-induced spreading and differentiation in embryonic stem cells. *Nat. Mater.* **9**, 82-88.

Darling, E. M., Topel, M., Zauscher, S., Vail, T. P. and Guilak, F. (2008). Viscoelastic properties of human mesenchymally-derived stem cells and primary osteoblasts, chondrocytes, and adipocytes. *J. Biomech.* **41**, 454-464.

Davidson, L. A. (2017). Mechanical design in embryos: mechanical signalling, robustness and developmental defects. *Philos. Trans. R. Soc. B Biol. Sci.* **372**, 20150516.

Di Carlo, D. (2012). A mechanical biomarker of cell state in medicine. *J. Lab. Autom.* **17**, 32-42.

Ekpenyong, A. E., Whyte, G., Chalut, K., Pagliara, S., Lautenschläger, F., Fiddler, C., Paschke, S., Keyser, U. F., Chilvers, E. R. and Guck, J. (2012). Viscoelastic properties of differentiating blood cells are fate- and function-dependent. *PLoS ONE* **7**, e45237.

Engler, A. J., Sen, S., Sweeney, H. L. and Discher, D. E. (2006). Matrix elasticity directs stem cell lineage specification. *Cell* **126**, 677-689.

Glaubitz, M., Medvedev, N., Pussak, D., Hartmann, L., Schmidt, S., Helm, C. A. and Delcea, M. (2014). A novel contact model for AFM indentation experiments on soft spherical cell-like particles. *Soft Mat.* **10**, 6732-6741.

Golfier, S., Rosendahl, P., Mietke, A., Herbig, M., Guck, J. and Otto, O. (2017). High-throughput cell mechanical phenotyping for label-free titration assays of cytoskeletal modifications. *Cytoskeleton* **74**, 283-296.

Gossett, D. R., Tse, H. T. K., Lee, S. A., Ying, Y., Lindgren, A. G., Yang, O. O., Rao, J., Clark, A. T. and Di Carlo, D. (2012). Hydrodynamic stretching of single cells for large population mechanical phenotyping. *Proc. Natl. Acad. Sci. USA* **109**, 7630-7635.

Guck, J., Schinkinger, S., Lincoln, B., Wottawah, F., Ebert, S., Romeyke, M., Lenz, D., Erickson, H. M., Ananthakrishnan, R., Mitchell, D. et al. (2005). Optical deformability as an inherent cell marker for testing malignant transformation and metastatic competence. *Biophys. J.* **88**, 3689-3698.

Guilak, F., Cohen, D. M., Estes, B. T., Gimble, J. M., Liedtke, W. and Chen, C. S. (2009). Control of stem cell fate by physical interactions with the extracellular matrix. *Cell Stem Cell* **5**, 17-26.

Guo, G., Yang, J., Nichols, J., Hall, J. S., Eyres, I., Mansfield, W. and Smith, A. (2009). Klf4 reverts developmentally programmed restriction of ground state pluripotency. *Development* **136**, 1063-1069.

Handorf, A. M., Zhou, Y., Halanski, M. A. and Li, W.-J. (2015). Tissue stiffness dictates development, homeostasis, and disease progression. *Organogenesis* **11**, 1-15.
Heisenberg, C.-P. and Bellaïche, Y. (2013). Forces in tissue morphogenesis and patterning. *Cell* **153**, 948-962.
Hussein, S. M. I., Puri, M. C., Tonge, P. D., Benevento, M., Corso, A. J., Clancy, J. L., Mosbergen, R., Li, M., Lee, D.-S., Cloonan, N. et al. (2014). Genome-wide characterization of the routes to pluripotency. *Nature* **516**, 198-206.
Lakes, R. (2009). Introduction: Phenomena. In *Viscoelastic Materials*, pp. 1-13. Cambridge: Cambridge University Press.
Lautenschläger, F., Paschke, S., Schinkinger, S., Bruel, A., Beil, M. and Guck, J. (2009). The regulatory role of cell mechanics for migration of differentiating myeloid cells. *Proc. Natl. Acad. Sci. USA* **106**, 15696-15701.
Lee, D.-S., Shin, J.-Y., Tonge, P. D., Puri, M. C., Lee, S., Park, H., Lee, W.-C., Hussein, S. M. I., Bleazard, T., Yun, J.-Y. et al. (2014a). An epigenomic roadmap to induced pluripotency reveals DNA methylation as a reprogramming modulator. *Nat. Commun.* **5**, 5619.
Lee, W. C., Shi, H., Poon, Z., Nyan, L. M., Kaushik, T., Shivashankar, G. V., Chan, J. K. Y., Lim, C. T., Han, J. and Van Vliet, K. J. (2014b). Multivariate biophysical markers predictive of mesenchymal stromal cell multipotency. *Proc. Natl. Acad. Sci. USA* **111**, E4409-E4418.
Li, R., Liang, J., Ni, S., Zhou, T., Qing, X., Li, H., He, W., Chen, J., Li, F., Zhuang, Q. et al. (2010). A mesenchymal-to-epithelial transition initiates and is required for the nuclear reprogramming of mouse fibroblasts. *Cell Stem Cell.* **7**, 51-63.
Lu, Y.-B., Franze, K., Seifert, G., Steinhäuser, C., Kirchhoff, F., Wolburg, H., Guck, J., Janmey, P., Wei, E.-Q., Käs, J. et al. (2006). Viscoelastic properties of individual glial cells and neurons in the CNS. *Proc. Natl. Acad. Sci. USA* **103**, 17759-17764.
Maherali, N., Sridharan, R., Xie, W., Utikal, J., Eminli, S., Arnold, K., Stadtfeld, M., Yachechko, R., Tchieu, J., Jaenisch, R. et al. (2007). Directly reprogrammed fibroblasts show global epigenetic remodeling and widespread tissue contribution. *Cell Stem Cell* **1**, 55-70.
Maître, J.-L., Turlier, H., Illukkumbura, R., Eismann, B., Niwayama, R., Nédélec, F. and Hiiragi, T. (2016). Asymmetric division of contractile domains couples cell positioning and fate specification. *Nature* **536**, 344-348.
Mammoto, T. and Ingber, D. E. (2010). Mechanical control of tissue and organ development. *Development* **137**, 1407-1420.
Mietke, A., Otto, O., Girardo, S., Rosendahl, P., Taubenberger, A., Golfier, S., Ulbricht, E., Aland, S., Guck, J. and Fischer-Friedrich, E. (2015). Extracting cell stiffness from real-time deformability cytometry: theory and experiment. *Biophys. J.* **109**, 2023-2036.
Mokbel, M., Mokbel, D., Mietke, A., Träber, N., Salvatore, G., Otto, O., Guck, J. and Aland, S. (2017). Numerical simulation of real-time deformability cytometry to extract cell mechanical properties. *ACS Biomater. Sci. Eng*.
Musah, S., Wrighton, P. J., Zaltsman, Y., Zhong, X., Zorn, S., Parlato, M. B., Hsiao, C., Palecek, S. P., Chang, Q., Murphy, W. L. et al. (2014). Substratum-induced differentiation of human pluripotent stem cells reveals the coactivator YAP is a potent regulator of neuronal specification. *Proc. Natl. Acad. Sci. USA* **111**, 13805-13810.
Neumann, K. (2014). H3K4 methyltransferases Mll1 and Mll2 have distinct roles and cooperate in neural differentiation and reprogramming. *PhD thesis*, Technische Universität Dresden, Dresden, Germany.
Nishioka, N., Inoue, K., Adachi, K., Kiyonari, H., Ota, M., Ralston, A., Yabuta, N., Hirahara, S., Stephenson, R. O., Ogonuki, N. et al. (2009). The hippo signaling pathway components lats and yap pattern Tead4 activity to distinguish mouse trophectoderm from inner cell mass. *Dev. Cell.* **16**, 398-410.
Ofek, G., Willard, V. P., Koay, E. J., Hu, J. C., Lin, P. and Athanasiou, K. A. (2009). Mechanical characterization of differentiated human embryonic stem cells. *J. Biomech. Eng.* **131**, 061011.
Ohnuki, M., Takahashi, K., Yamanaka, S., Ohnuki, M., Takahashi, K. and Yamanaka, S. (2009). Generation and characterization of human induced pluripotent stem cells. In *Current Protocols in Stem Cell Biology*, pp. 4A.2.1-4A.2.25. Hoboken, NJ, USA: John Wiley & Sons, Inc.
Otto, O., Rosendahl, P., Mietke, A., Golfier, S., Herold, C., Klaue, D., Girardo, S., Pagliara, S., Ekpenyong, A., Jacobi, A. et al. (2015). Real-time deformability cytometry: on-the-fly cell mechanical phenotyping. *Nat. Methods.* **12**, 199-202.
Pajerowski, J. D., Dahl, K. N., Zhong, F. L., Sammak, P. J. and Discher, D. E. (2007). Physical plasticity of the nucleus in stem cell differentiation. *Proc. Natl. Acad. Sci. USA* **104**, 15619-15624.
Panciera, T., Azzolin, L., Fujimura, A., Di Biagio, D., Frasson, C., Bresolin, S., Soligo, S., Basso, G., Bicciato, S., Rosato, A. et al. (2016). Induction of expandable tissue-specific stem/progenitor cells through transient expression of YAP/TAZ. *Cell Stem Cell* **19**, 725-737.
Panciera, T., Azzolin, L., Cordenonsi, M. and Piccolo, S. (2017). Mechanobiology of YAP and TAZ in physiology and disease. *Nat. Rev. Mol. Cell Biol*.
Pillarisetti, A., Desai, J. P., Ladjal, H., Schiffmacher, A., Ferreira, A. and Keefer, C. L. (2011). Mechanical phenotyping of mouse embryonic stem cells: increase in stiffness with differentiation. *Cell. Reprogram.* **13**, 371-380.
Polo, J. M., Anderssen, E., Walsh, R. M., Schwarz, B. A., Nefzger, C. M., Lim, S. M., Borkent, M., Apostolou, E., Alaei, S., Cloutier, J. et al. (2012). A molecular roadmap of reprogramming somatic cells into iPS cells. *Cell* **151**, 1617-1632.
Przybyla, L., Lakins, J. N. and Weaver, V. M. (2016). Tissue mechanics orchestrate Wnt-dependent human embryonic stem cell differentiation. *Cell Stem Cell* **19**, 462-475.
R Core Team (2017). R: A language and environment for statistical computing. R Foundation for Statistical Computing, Vienna, Austria, www.R-project.org/.
Rosendahl, P., Plak, K., Jacobi, A., Kraeter, M., Toepfner, N., Otto, O., Herold, C., Winzi, M., Herbig, M., Ge, Y. et al. (2017). Real-time fluorescence and deformability cytometry — flow cytometry goes mechanics. *bioRxiv*. doi:10.1101/187435
Sakurai, K., Talukdar, I., Patil, V. S., Dang, J., Li, Z., Chang, K.-Y., Lu, C.-C., Delorme-Walker, V., Dermardirossian, C., Anderson, K. et al. (2014). Kinome-wide functional analysis highlights the role of cytoskeletal remodeling in somatic cell reprogramming. *Cell Stem Cell* **14**, 523-534.
Samavarchi-Tehrani, P., Golipour, A., David, L., Sung, H.-K., Beyer, T. A., Datti, A., Woltjen, K., Nagy, A. and Wrana, J. L. (2010). Functional genomics reveals a BMP-Driven mesenchymal-to-Epithelial transition in the initiation of somatic cell reprogramming. *Cell Stem Cell* **7**, 64-77.
Scarcelli, G., Polacheck, W. J., Nia, H. T., Patel, K., Grodzinsky, A. J., Kamm, R. D. and Yun, S. H. (2015). Noncontact three-dimensional mapping of intracellular hydromechanical properties by Brillouin microscopy. *Nat. Methods.* **12**, 1132-1134.
Shakiba, N., White, C. A., Lipsitz, Y. Y., Yachie-Kinoshita, A., Tonge, P. D., Hussein, S. M. I., Puri, M. C., Elbaz, J., Morrissey-Scoot, J., Li, M. et al. (2015). CD24 tracks divergent pluripotent states in mouse and human cells. *Nat. Commun.* **6**, 7329.
Silva, J., Barrandon, O., Nichols, J., Kawaguchi, J., Theunissen, T. W. and Smith, A. (2008). Promotion of reprogramming to ground state pluripotency by signal inhibition. *PLoS Biol.* **6**, 2237-2247.
Sneddon, I. N. (1965). The relation between load and penetration in the axisymmetric boussinesq problem for a punch of arbitrary profile. *Int. J. Eng. Sci.* **3**, 47-57.
Sun, Y., Yong, K. M. A., Villa-Diaz, L. G., Zhang, X., Chen, W., Philson, R., Weng, S., Xu, H., Krebsbach, P. H. and Fu, J. (2014). Hippo/YAP-mediated rigidity-dependent motor neuron differentiation of human pluripotent stem cells. *Nat. Mater.* **13**, 599-604.
Takahashi, K. and Yamanaka, S. (2006). Induction of pluripotent stem cells from mouse embryonic and adult fibroblast cultures by defined factors. *Cell* **126**, 663-676.
Tan, Y., Kong, C., Chen, S., Cheng, S. H., Li, R. A. and Sun, D. (2012). Probing the mechanobiological properties of human embryonic stem cells in cardiac differentiation by optical tweezers. *J. Biomech.* **45**, 123-128.
Tonge, P. D., Corso, A. J., Monetti, C., Hussein, S. M. I., Puri, M. C., Michael, I. P., Li, M., Lee, D.-S., Mar, J. C., Cloonan, N. et al. (2014). Divergent reprogramming routes lead to alternative stem-cell states. *Nature* **516**, 192-197.
Wozniak, M. A. and Chen, C. S. (2009). Mechanotransduction in development: a growing role for contractility. *Nat. Rev. Mol. Cell Biol.* **10**, 34-43.
Xu, W., Mezencev, R., Kim, B., Wang, L., McDonald, J. and Sulchek, T. (2012). Cell stiffness is a biomarker of the metastatic potential of ovarian cancer cells. *PLoS ONE* **7**, e46609.
Yim, E. K. F. and Sheetz, M. P. (2012). Force-dependent cell signaling in stem cell differentiation. *Stem Cell Res. Ther.* **3**, 41.
Ying, Q.-L., Stavridis, M., Griffiths, D., Li, M. and Smith, A. (2003). Conversion of embryonic stem cells into neuroectodermal precursors in adherent monoculture. *Nat. Biotechnol.* **21**, 183-186.
Ying, Q.-L., Wray, J., Nichols, J., Batlle-Morera, L., Doble, B., Woodgett, J., Cohen, P. and Smith, A. (2008). The ground state of embryonic stem cell self-renewal. *Nature* **453**, 519-523.
Yu, H., Tay, C. Y., Leong, W. S., Tan, S. C. W., Liao, K. and Tan, L. P. (2010). Mechanical behavior of human mesenchymal stem cells during adipogenic and osteogenic differentiation. *Biochem. Biophys. Res. Commun.* **393**, 150-155.
Zhu, G. and Trung Nguyen, N. (2010). Particle sorting in microfluidic systems. *Micro Nanosyst.* **2**, 202-216.